Histol Histopathol (2009) 24: 1367-1379
DOI: 10.14670/HH-24.1367

http://www.hh.um.es

Histology and Histopathology
Cellular and Molecular Biology

Lymphatic spread of mesenchymal renal tumor to metastatic parathymic lymph nodes in rat

David Rozsa[1], Gyorgy Trencsenyi[1], Pal Kertai[2], Terez Marian[3], Gabor Nagy[1] and Gaspar Banfalvi[1]

[1]Department of Microbial Biotechnology and Cell Biology, [2]Institute of Preventive Medicine and [3]Department of Nuclear Medicine, University of Debrecen, Debrecen, Hungary

Summary. Rat mesenchymal renal tumor cells (NeDe) transplanted under the kidney capsule of F344 rats resulted in metastases in the parathymic lymph nodes. Tumor cells were isolated from these tumor-bearing lymph nodes and 10^6 cells were implanted under the kidney capsule. Tumor growth after this implantation could be traced within six days. India ink was implanted to prove that there is a connection between the lymphatic vessels of the kidney capsule and the parathymic lymph nodes. The distribution of the radioligand ^{18}FDG in different organs also provided evidence that the parathymic lymph nodes are the primary sites of metastatic tumor growth. Tumor growth was followed after staining sections of biopsies of normal, tumorous kidneys and parathymic lymph nodes embedded in paraffin. The progression of tumor formation was seen as a frontline between the healthy and tumor bearing tissue. This demarcation line was sharp at the beginning of the invasion and at the peripheral regions of the tumor, while the central region infiltrated into the healthy kidney tissue. The initial invasion gradually turned to an infiltration resulting in the disruption of the renal tissue, especially at the periphery. Accumulation of lipids and flow of blood to the lymphatic vessels was due to the lack of angiogenesis, leading to an increased pressure of the interstitial fluid. Interstitial damage ultimately led to the appearance of blood and the growth of tumor cells in parathymic lymph nodes. The kidney capsule-parathymic lymph node complex is proposed as a suitable metastatic model for the isolated *in vivo* examination of tumor development and for the analysis of secondary tumors.

Offprint requests to: Prof. Gaspar Banfalvi Ph.D., D.Sc., University of Debrecen, 1 Egyetem Square, Debrecen 4010, Hungary. e-mail: bgaspar@delfin.klte.hu

Key words: Renal tumor, NeDe cell line, Arterial-lymphatic shunt, Metastasis model

Introduction

As the tumor progresses it becomes more autonomous and uncontrollable (Guyton and Kensler, 1993). This stage is known as the metastatic development of cancer, namely the spead of tumor cells from the primary site to distant parts of the body. Contrary to the successful removal or therapy of the primary tumor, the grave prognosis of patients with metastasis remains the most significant problem of cancer research. Due to the complexity of metastatic development it is difficult to predict at which step the cascade succumbs or explodes, consequently not much is known how the tumor formation turns to a metastatic process.

Nitrosamines, including N-dimethylnitrosoamine are present in food, tobacco smoke, and in different environmental sources (Diaz Gomez et al., 1986), thus their constant presence underlines the prognostic relevance for patients with renal carcinoma. The comparison of the histology of neoplasm of the rat kidney conforming to the classification of nephroblastoma with that of N-nitrosodimethylamine-induced renal mesenchymal tumors revealed separate morphologic characteristics, and the unrelated existence of rat nephroblastoma and renal mesenchymal tumor. The rat nephroblastoma morphologically resembles not only the malignant epithelial component of human Wilms' tumor, but also, the rat renal mesenchymal tumor appeared to have counter-parts in the mesenchymal component of Wilms' tumor (Hard and Grasso, 1976). Indeed, when the classification of several kidney tumors was attempted, considerable overlaps were found

(Marsden and Newton, 1986). In conformity with this ambiguity the existence of two different types of metastatic renal cell carcinoma tumor models has been proposed (Delahunt and Eble, 1997; Delahunt et al., 2001). Type 1 consists of small cells (Jiang et al., 1998), and type 2, having large eosinophilic cells, which occur more commonly in younger patients associated with more aggressive characteristics and with worse prognosis (Ono et al., 1997; Jiang et al., 1998; Delahunt et al., 2001). None of the renal tumor models made distinction between type 1 and type 2 subgroups (Delahunt and Eble, 1997).

Contrary to the establishment of several tumor models (Otto et al., 1984a,b; Guha et al., 1991; Grossi et al., 1992; Hillman et al., 1994; Angevin et al., 1999; Pulkkanen et al., 2000) the number of metastatic renal models remained rare (Rowe et al., 1999; Zisman et al., 2003). The chorioallantois-membrane system of chicken embryos, the implantation of primary tumors of rodents, the implantation of heterogeneous tumors into immuno-deficient rodents, and the intravenous injection of tumors are regarded as such models (Fidler and Nicholson, 1987; Hill, 1992; Hart and Saini, 1992; Welch, 1997; Khanna and Hunter, 2005). Renal mesenchymal tumors were induced by N-dimethylnitrosamine (Magee and Barnes, 1962). A single intraperitoneal injection of a metastatic dose (60 mg/kg) of N-dimethylnitrosamine in rats induced 100% incidence of mesenchymal renal tumors. Additionally in about 30% of the animals adenocarcinoma development was observed (Magee and Barnes, 1962; Thomas and Schmahl, 1964; Swann and McLean, 1968; Jasmin and Riopelle, 1968; Hard and Butler, 1970). None of these tumor models made distinction between type 1 and type 2 subgroups (Delahunt and Eble, 1997).

The reaction of adult and newborn rats upon the administration of a single metastatic dose of intravenous N-nitrosodimethylamine was different. Mesenchymal tumors were predominantly associated with the newborn rat, while adenocarcinomas and mesenchymal tumors with equal frequency occurred when the same carcinogenic dose was injected into immature or adult rats (Terracini and Magee, 1964; Murphy et al., 1966). The analysis of the fine structure of renal tumor cells has shown persisting lesions in the primary tumor, which consisted primarily of aggregations of fibroblast-like cells (Hard and Butler, 1971a; Hard, 1985). Although, mesenchymal mesoblastic nephroma primary tumors are considered benign tumors, the neoplasm induced with N-dimethynitrosoamine was characterized as an embryonal sarcoma of the kidney and regarded as an aggressive, malignant mesenchymal renal tumor (Hard and Butler, 1970; Hard and Butler, 1971a,b).

Earlier, we implanted a known number of tumor cells obtained by N-dimethylnitrosamine treatment under the kidney capsule by means of Gelaspon® gelatin sponge and followed the kinetics of tumor growth (Uzvolgyi et al., 1990). During these experiments both the expansion of mesenteric lymph nodes and the initiation of angiogenesis were observed. This led to the recognition that tumor growth was paralleled by the infiltration of parathymic lymph nodes and an increased activity of pyruvate kinase (Paragh et al., 2005). Our observation that tumor cells appeared first in the abdominal primary tumor then in thoracal lymph nodes indicated metastasis formation. The question is of clinical importance, how the tumor cells move from the subrenal capsule to the parathymic glands. Related to the infiltration of tumor cells from the kidney to the parathymic lymph nodes this paper describes that the kidney-capsule parathymic lymph node system is a suitable tool as a metastatic tumor model.

Materials and methods

Materials

All chemicals were of analytical or spectroscopic grade. Collagenase type I, hyaluronidase type IV, DNase type I, trypsin, penicillin, streptomycin, cytochalasin B were purchased from Sigma-Aldrich Kft (Budapest, Hungary). Growth media, gentamicin and serum were obtained from GIBCO BRL, Life Technologies (Gaithersburg, MD). The method of Hamacher et al. (1986) was used to prepare the radiotracer positron emitting glucose analog 2-[^{18}F]fluoro-2-deoxy-D-glucose (^{18}FDG) which has a relatively convenient half life of 109.74 min. The synthesis and labeling with the positron decaying isotope ^{18}F took place in the Center for Positron Emission Tomography (Debrecen, Hungary).

Solutions

The Hank's buffered salt solution (HBSS) contained 137 mM NaCl, 5.4 mM KCl, 0.25 mM Na_2HPO_4, 0.44 mM KH_2PO_4, 1.3 mM $CaCl_2$, 1.0 mM $MgSO_4$ and 4.2 mM $NaHCO_3$. Phosphate buffered saline (PBS) contained 140 mM NaCl, 5 mM KCl, 8 mM Na_2HPO_4, 3 mM NaH_2PO_4, pH 7.4.

Animals

In each experiment three adult female Fischer 344 (F344) rats, weighting 150-200 g, were used unless otherwise noted. Rats were kept in a conventional laboratory environment and fed on a semi-synthetic diet (Charles River Mo, Kft, Godollo, Hungary) and tap water *ad libitum*. Animals received human care to the criteria outlined in the "Guide for the Care and Use of Laboratory Animals" (Workman et al., 1988), authorized by the Ethical Committee for Animal Research, University of Debrecen, Hungary (permission number: 22/2007).

Experimental tumor

We have used the mesenchymal mesoblastic

nephroma (Nephroma Debreceniensis, NeDe) isolated from Fischer 344 rats which were treated at newborn age by injecting i.p. 125 μg/animal N-nitroso-dimethylamine (Sigma-Aldrich Kft, Budapest, No 77561) in saline. Kidney tumors were removed 5-7 months after chemical tumorogenesis, minced into smaller pieces and tumor slices were frozen (Dezso et al., 1991; Paragh et al., 2003; Trencsenyi et al., 2007).

N-nitrosodimethylamine is found in the National Prioritities List containing more than one thousand sites identified by the Environmental Protection Agency. It causes liver, kidney, and lung cancers in animals. The European Union legislation considers nongenotoxic substances that only cause liver tumors in certain sensitive strains of rats as raising no concern for man. However, this does not mean that N-nitrosodimethylamine would not be toxic to other animals or man. The Department of Health and Human Services has determined that N-nitrosodimethylamine may be reasonably anticipated to be a human carcinogen. Toxicity data, including N-nitrosodimethylamine, can be found at the Agency for Toxic Substances and Disease Registry (www.atsdr.cdc.gov/toxfaq.html).

Establishment of tumor cell lines

Freshly isolated kidney tumors or tumor slices frozen in liquid nitrogen were minced into 2x2x2 mm pieces, incubated for 3 h at 37°C in RPMI 1640 medium containing 100 mg collagenase I, 10 mg hyaluronidase and 30 μl DNase I in 100 ml. After digestion the mixture was filtered through four layers of sterile gauze, washed and resuspended in RPMI 1640 medium supplemented with 10% FBS and antibiotics. After overnight incubation at 37°C in 5% carbon dioxide (CO_2) atmosphere, nonadherent cells were discarded and adherent cells were subcultured. The primary cell culture was continuously grown and after a further 20 daily subculturings the new cell line was established, frozen in liquid nitrogen and used for further experiments. NeDe cell line was used as an exponentially growing monolayer culture (37°C, 5% CO_2), maintained by daily passage in RPMI 1640 supplemented with 10% FBS, 100 U/ml penicillin, and 100 μg/ml streptomycin. Cell viability was more than 95%, as assessed by trypan blue exclusion.

Experimental surgery

The aim of the surgical operations was to place Gelaspon® discs under the capsule of the left kidney. To transplant cells or India ink, gelatin sponge discs of 4 mm diameter and 1 mm thickness were cut from Gelaspon® plates and sterilized. The movement of tumor cells from the renal capsule to the parathymic lymph nodes was mimicked by dropping India ink on the Gelaspon® disc and implanting it under the capsule of the left kidney of F344 rats. This experiment was similar to the implantation of tumor cells. When India ink was transplanted, 10 μl Pelikan ink (Gunther Wagner, Pelikan Werke, Hannover) was placed on the gelatin disc. For the transplantation of tumor cells NeDe cells (10^6) in 10 μl were dropped on the Gelaspon® disc. Experimental animals were anesthesized by i.p. administration of 3 mg/100g pentobarbital (Nembutal). The abdominal cavity was opened, the kidney was pulled out and the India ink or tumor cell containing disc was placed under the renal capsule. Stitches were put in the wound, autopsy and experiments were carried out two weeks later.

Organ-distribution

On day 14 after implantation, control and tumor-bearing rats were anesthetized and the radioligand ^{18}FDG (15 MBq in 1 ml saline) was injected into the left femoral vein of each rat. Animals were euthanized 60 min after ^{18}FDG administration with 300 mg/kg pentobarbital. Blood samples were taken from the aorta to determine the activity of the plasma. Tissue samples were taken from liver, kidney, abdominal muscle and from the tumor. The whole thymus and parathymic lymph nodes were removed. The weight and the radioactivity of the samples were used to determine the differential absorption ratio (DAR).
DAR was calculated as:

$$DAR = \frac{\text{(accumulated radioactivity/g tissue)}}{\text{(total injected radioactivity/body weight)}}$$

Tissue staining

Delafield's hematoxylin has been used to stain nuclei and ribosomes as a deep blue-purple complex formed with negatively charged nucleic acids and eosin to stain proteins pink nonspecifically. Differentiation of staining was done in dilute acid alcohol (due to hematoxylin's greater solubility in alcohol). Differentiation was stopped by washing the slides in water. Sudan black B was used to stain lipid droplets.

Statistical analysis

Statistical analysis was performed with 2-way ANOVA and Student's t test. Results were expressed as mean ± standard deviation (SD) (n=3), $p<0.01$ was considered significant.

Results

Tumor cell infiltration in the kidney

Gelatin disc containing NeDe tumor cells (10^6) were implanted under the left renal capsule. F344 rats were euthanized and the tumor development was registered by measuring the weight of the left kindneys that were removed and freed from the fat tissue after 3, 6 and 12

days, weighing 0.72, 0.92 and 5.32 g, respectively. In the control experiment saline containing Gelaspon® disc was implanted. The average weight of the kidneys of these control rats was 0.62 g three days after implantation. The morphology of the control and tumor-bearing kidneys is shown in Fig. 1.

The control shows a normal kidney with the Gelaspon® disc (Fig. 1a). After 3 days of tumor cell infiltration the kidney surface differed from the surface of the control indicating the beginning of tumorogenesis (Fig. 1b). Although tumor vascularization was not visible, the Gelaspon was shrinking, due to the absoption of the gelatin. Six days after tumor cell implantation the weight of the left kidney was almost 50% higher, containing distinguishable tumors (Fig. 1c). After 12 days of tumor cell implantation the tumor which started to grow first outward on the surface of the kidney to the direction of the lower pressure, infiltrated into the kidney causing its complete destruction (Fig. 1d). Tumor infiltration into the kidney started at the place of gelatin disc implantation at the tumor-kidney border. Often, a sharp demarcation line divided the healthy and neoplastic tissue (Fig. 2).

Appearance of red blood cells in disrupted primary tumor

At day 3 after tumor cell implantation under the renal capsule the hematoxylin-eosin staining of kidney tissue did not reveal significant changes (Fig. 3a) and eosinophil enhanced staining of the tumor infiltration did not show the presence of red blood cells (Fig. 3b). By day 12 the tumor size increased enormously and the invaded kidney tissue was destroyed, with some of its elements (glomerules, tubules) still recognizable. Several ruptures were seen and the substance of the tumor disintegrated as shown by hematoxylin-eosin staining (Fig. 3c). Eosinophil areas contained many red blood cells (Fig. 3d).

Appearance of red blood cells in parathymic lymph nodes

The same hematoxylin staining was used to trace the presence or absence of red blood cells in parathymic

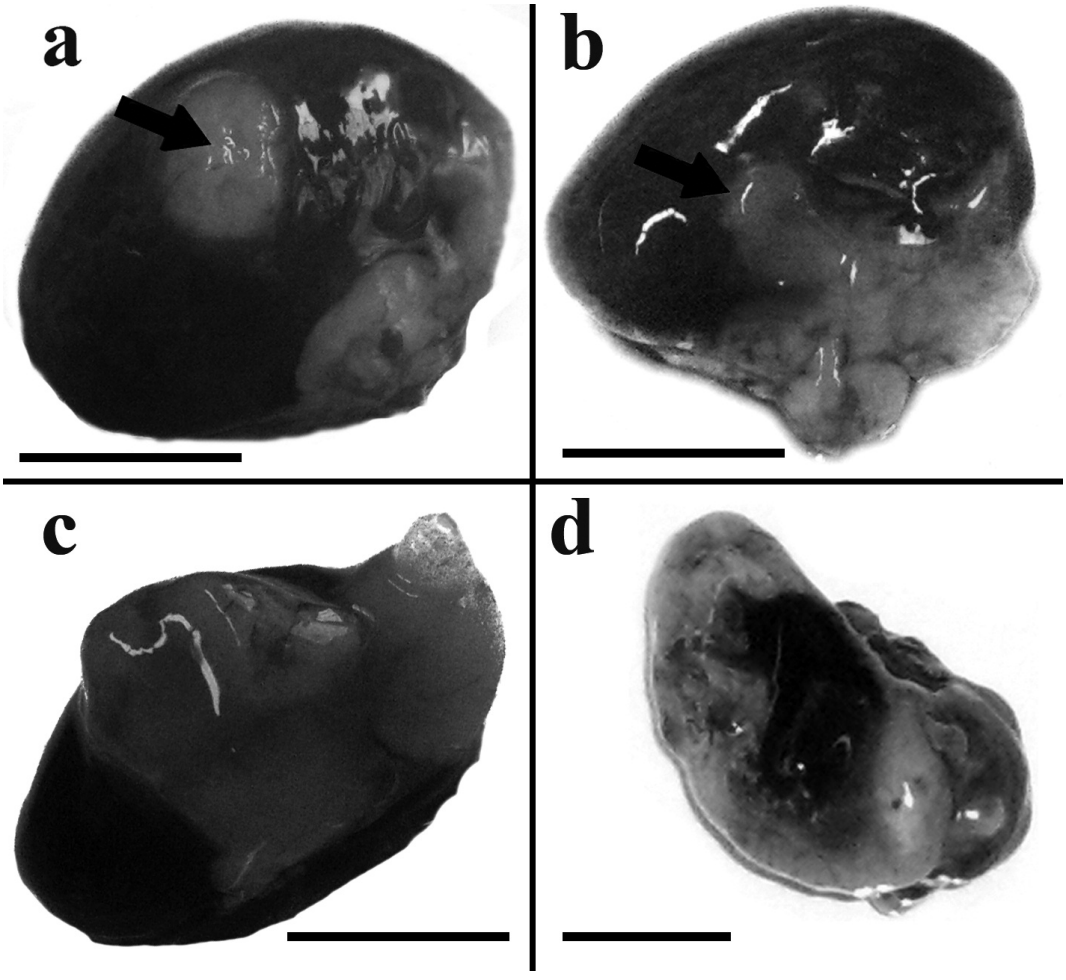

Fig. 1. Development of primary tumor after NeDe cell implantation. **a.** Control kidney one day after gelatin sponge implantation. Tumor formation after: 3 days **(b)**, 6 days **(c)** and 12 days **(d)**. Black arrows point to the implanted white Gelaspon® disc. Bar: 1 cm

lymph nodes after tumor cell implantation. In the control lymph nodes there were no red blood cells (Fig. 4a,b). At day 12 after tumor cell implantation hematoxylin-eosin stained tissue disruptions were seen in the parathymic lymph nodes (Fig. 4c). The enhancement of the eosinophil staining revealed the presence of aggregations of red blood cells (Fig. 4d).

Visualizing the stream of tissue fluid after gelatin disc implantation

Collagen, which is the source of gelatin, is known to strengthen blood vessels and plays a role in tissue development. Therefore we thought that the transient vascularization could be initiated by the gelatin hydrogel of the implanted Gelaspon® disc. But before vascularization could have been taken place in the tumor, gelatin fibres appeared in the kidney 3 days after Gelaspon® implantation, showing the stream of the absorbed gelatin in the interstitial fluid (Fig. 5). As the tumor cells on the surgical gelatin sponge were directed toward the kidney, these cells attached to the surface of the kidney, serving as a basis of the invasion through the demarcation zone. The appearance of gelatin fibers not only indicates the flow of tissue fluid, but is also likely to determine the main stream of tumor cells from the gelatin disc.

Lipid accumulation in the primary tumor

The high level of "aerobic glycolysis" in primary tumors was explained by the glucose-citrate-lipogenesis pathway (Medes et al., 1953; Parlo and Coleman, 1984; Parlo and Coleman, 1986; Costello and Franklin, 2005). If this was the case also in the mesenchymal primary tumor, then under hypoxic conditions one would expect the accumulation of acetylcoenzyme A. The excess acetylcoenzyme A could be shunted to other pathways, such as fatty acid and lipid synthesis. To confirm that this pathway is activated, lipid droplet formation in the primary tumor after 6 days of implantation of tumor cells was visualized by Sudan black staining. Fig. 6 shows the presence of large lipid droplets in the primary tumor, confirming the notion of a high glycolytic activity and lipid formation.

Appearance of tumor cells in parathymic lymph nodes

The NeDe cell line (10^6 cells/ rat) placed under the renal capsule resulted not only in local mesenchymal tumor, but also in lymph node tumor in parathymic lymph nodes (PTNs) (Fig. 7). This was confirmed by the

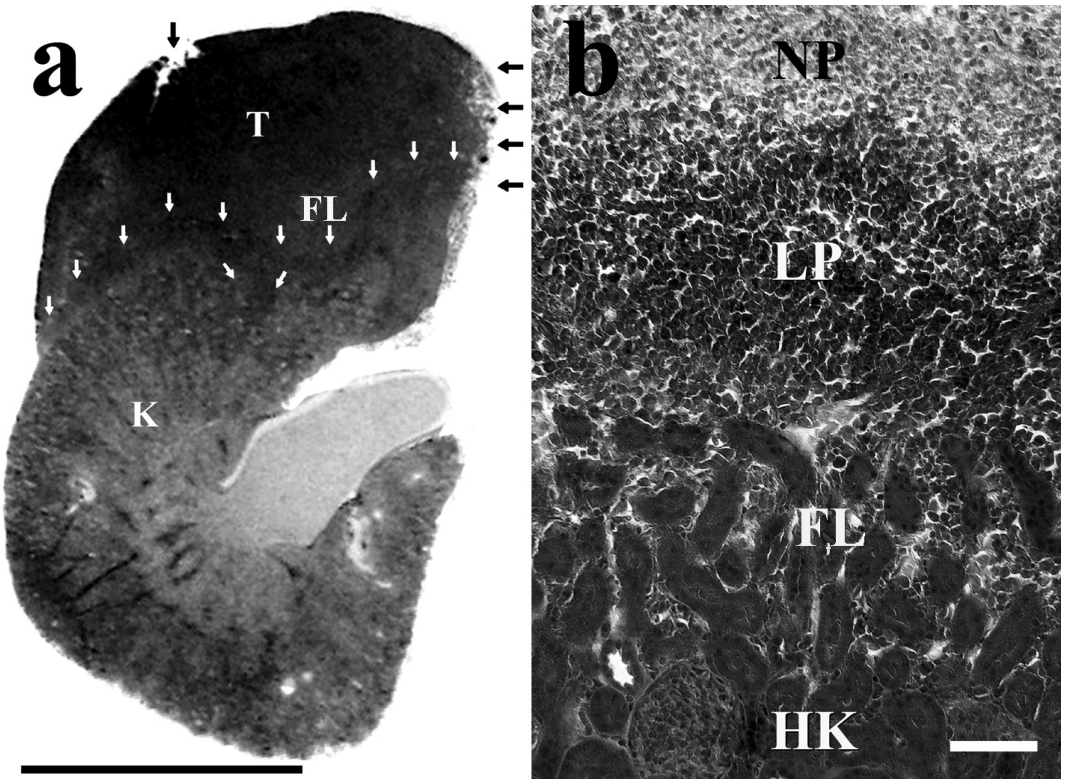

Fig. 2. Tumor formation after 12 days of NeDe cell implantation under the left subrenal capsule of rat. **a.** Tumor formation (upper part), kidney (lower part). Black arrows indicate tumor disruptions, white arrows the frontline. **b.** Tissue section of tumor-bearing kidney. T, tumor; NP, necrotic part of tumor; LP, living part of tumor; FL, frontline; K, kidney; HK, healthy kidney. Hematoxylin-eosin staining. Bars: a, 1 cm; b 100 μm.

subcapsular implantation of tumor-bearing PTNs in rats and by the observation that six-day-old PTN implants induced tumor gowth (Trencsenyi et al., 2009). While the control lymph node is healthy and small (Fig. 7a), the PTNs were enlarged 6 days after the subcapsular placement of tumor cells (Fig. 7b).

Transport of abdominal ink particles to thoracal parathymic lymph nodes

Control animals received saline containing gelatin sponge. Six hours after implantation rats were euthanized and their parathymic lymph nodes were removed. The tissue sections of parathymic lymph nodes are visualized in Fig. 8. The control lymph node (Fig. 8a) and control kidney (Fig. 8c) are healthy and small. Six hours after its implantation the ink appeared not only in the kidney (Fig. 8d), but also in parathymic lymph nodes (Fig. 8b). The appearance of India ink in PTNs is shown at higher magnification in the tissue section of the parathymic lymph node (Fig. 8e). Control lymph nodes did not contain ink. Since India ink could not be traced in other lymph nodes, it was concluded that parathymic lymph nodes were the primary targets in this metastatic rat model.

Metastatic potential of tumor cells in different tissues

The metastatic tumor spread was supported by experiments related to tissue metabolism carried out in six female F344 rats. After 14 days of subcapsular transplantation of NeDe cells, animals were given

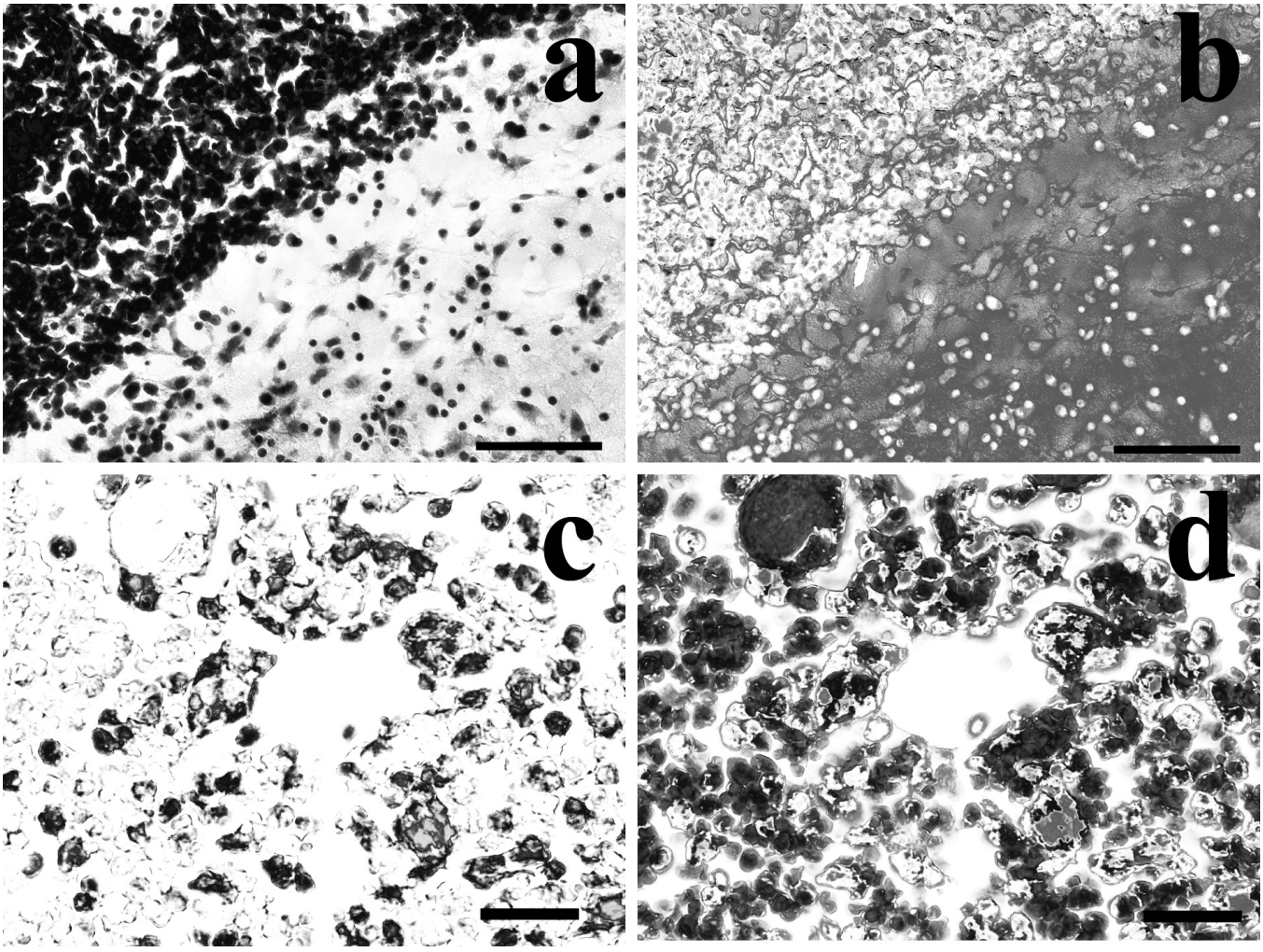

Fig. 3. Tumor infiltration in kidney at days 3 and 12 after tumor cell implantation. **a.** Hematoxylin-eosin staining of the kidney tissue at day 3. **b.** enhancement of the eosinophil part of the hematoxylin-eosin staining of the same tissue section at day 3. **c.** Enhancement of the basophil part of the hematoxylin-eosin staining at day 12. **d.** Enhancement of eosynophyl parts of **c** with dark clusters of red blood cells. Bar: 100 μm.

intravenously 15.0 MBq ^{18}FDG in saline. After 1 h animals were euthanized and blood samples were taken from the aorta. The tumor, liver, kidney, thymus and the abdominal rectal muscle (*musculus rectus abdominalis*) and the parathymic lymph nodes were removed. Three tissue samples were taken from each organ and from parathymic glands and their activities were measured with a gamma counter. Figure 9 contains the distribution of ^{18}FDG radioactivity expressed in DAR values in different organs in the control and in NeDe tumor-bearing rats. The DAR value of NeDe tumor was 11-times and the parathymic lymph nodes 9-times higher than that of the muscle (Fig. 9), supporting the notion that parathymic glands are involved in metastatic tumor growth. The DAR values of blood and other tissues of tumor-bearing animals did not differ significantly from those of control samples taken from healthy rats.

Discussion

Recently, we have implanted hepatocellular tumor cells (HeDe) under the renal capsule of rats and extremely enlarged lymph nodes near the tumor-infiltrated liver were found two weeks later. These lymph nodes turned out to be the parathymic lymph nodes (Trencsenyi et al., 2007). This observation raised the question whether mesenchymal renal tumor (NeDe) cells have a similar metastatic effect. The method of implanting tumors under the kidney capsule was established for the fast screening of chemotherapeutic agents (Bogden et al., 1979). The application of the kidney capsule method allowed us to follow the dynamics of isogenic tumor growth (Uzvolgyi et al., 1990). In the course of these experiments, changes in the parathymic lymph nodes and the presence of tumor cells

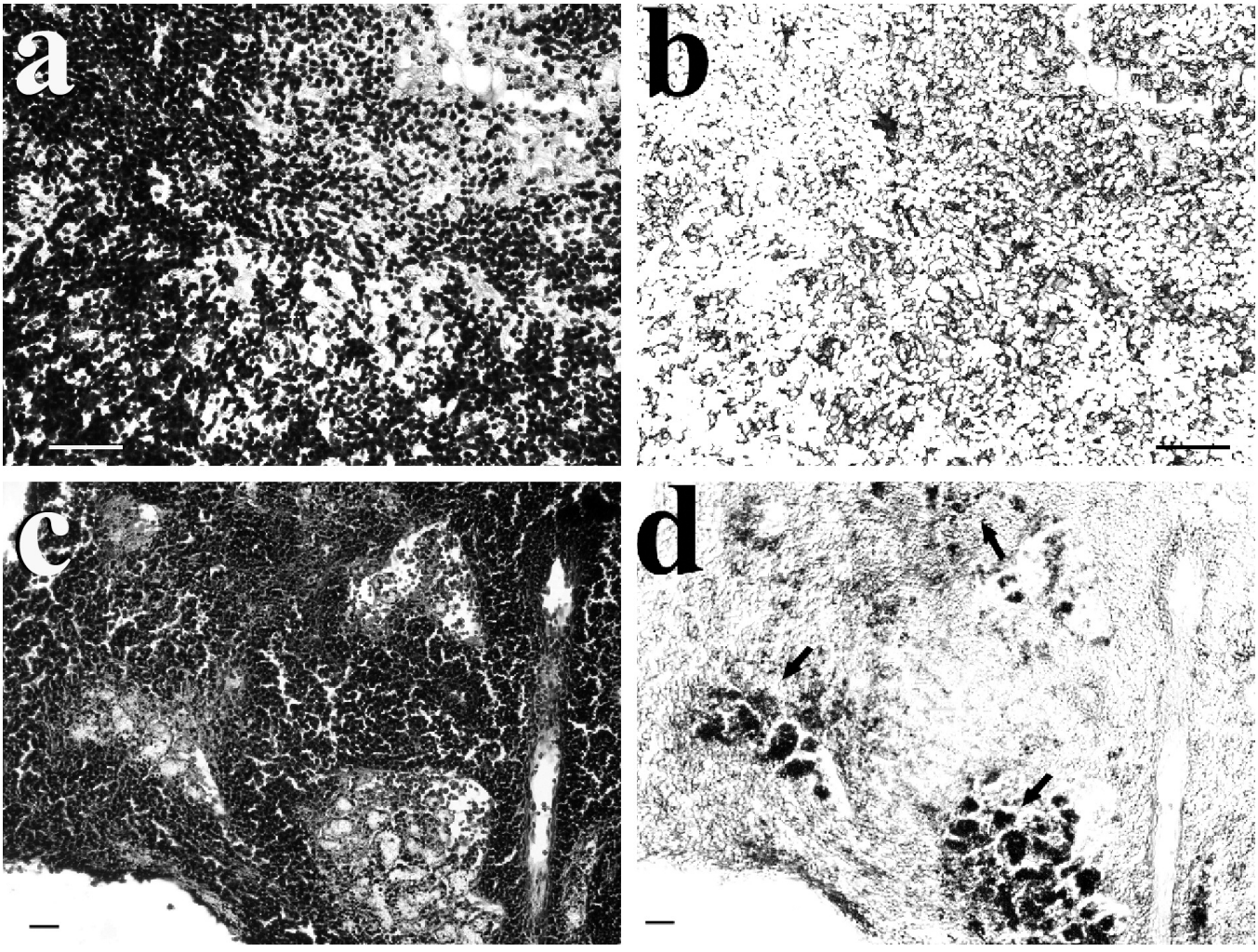

Fig. 4. Tumor infiltration in parathymic lymph nodes at day 12 after tumor cell implantation. **a.** Control, healthy lymph node after hematoxylin staining. **b.** enhancement of the eosinophil part of the hematoxylin staining of the same tissue section. **c.** Hematoxylin staining of tumor-bearing PTNs at day 12. **d.** Enhancement of eosynophyl parts of **c** with dark clusters of red blood cells indicated by the black arrows. Bar: 100 μm.

in these glands have been observed by histological examinations (Paragh et al., 2005).

Metastases from solid tumors occur through the dissemination of tumor cells in the bloodstream and lymphatic system. It is known that lymph node infiltration has become important for identifying patients

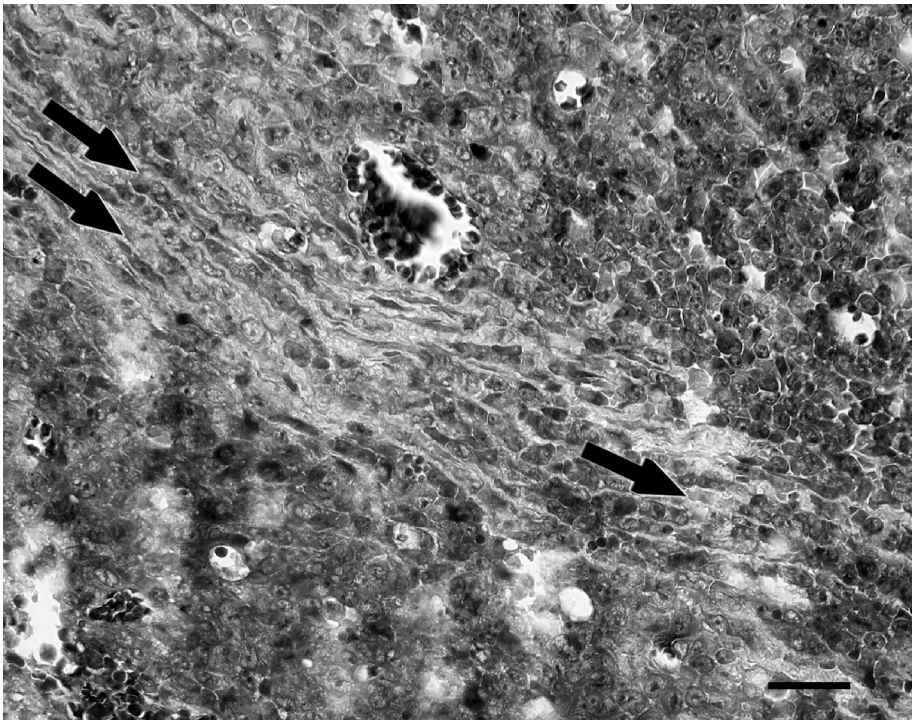

Fig. 5. The appearance of gelatin fibers indicating the main stream of interstitial fluid flow in kidney tissue three days after gelatin disc implantation. Staining: hematoxylin/eozin. Bar: 50 μm.

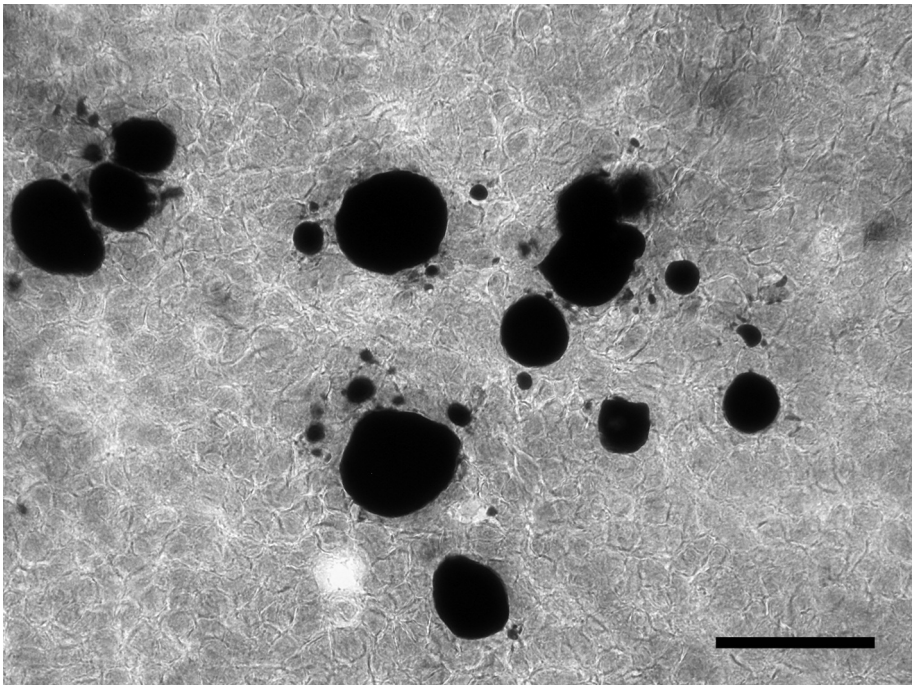

Fig. 6. Lipid droplets in primary tumor six days after tumor cell implantation. Staining: Sudan black B. Bar: 50 μm.

with breast cancer or malignant melanoma. However, the identification of tumor cells in lymph nodes may escape detection (Zoli et al., 2002). To avoid such a possibility the radiotracer 2-fluoro-[^{18}F]-2-deoxi-D-glucose (^{18}FDG) was injected in tumor-bearing rats and its accumulation was followed in different tissues. High levels of radiotracer were detected in the tumor and in parathymic lymph nodes, while in other tissues and organs (blood, liver, muscle, thymus) the distribution of the radiotracer was similar to the control animals. Further confirmation that mesenchymal renal tumor cells (NeDe) implanted under the subcapsule of the kidney

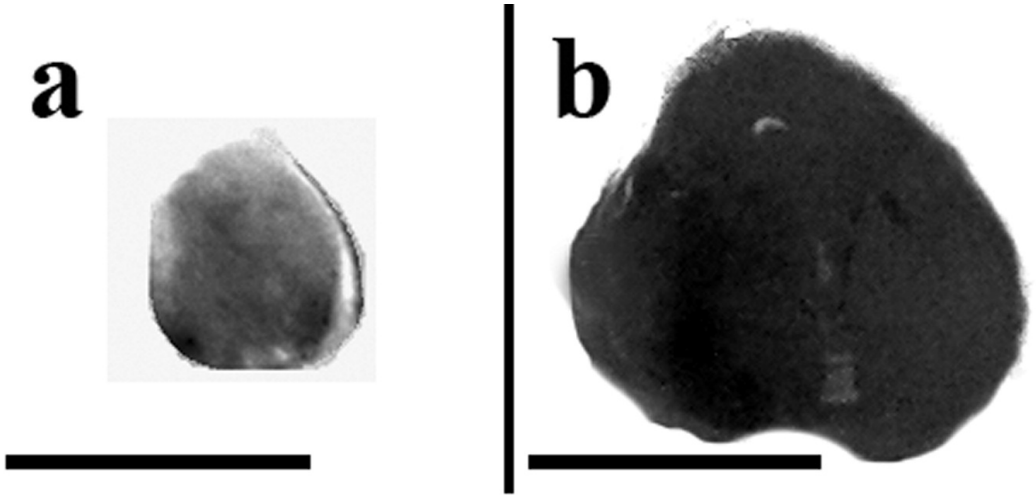

Fig. 7. Enlargement of parathymic lymph nodes six days after tumor cell implantation. **a.** control PTN, **b.** tumor-bearing PTN. Bar: 0.5 cm.

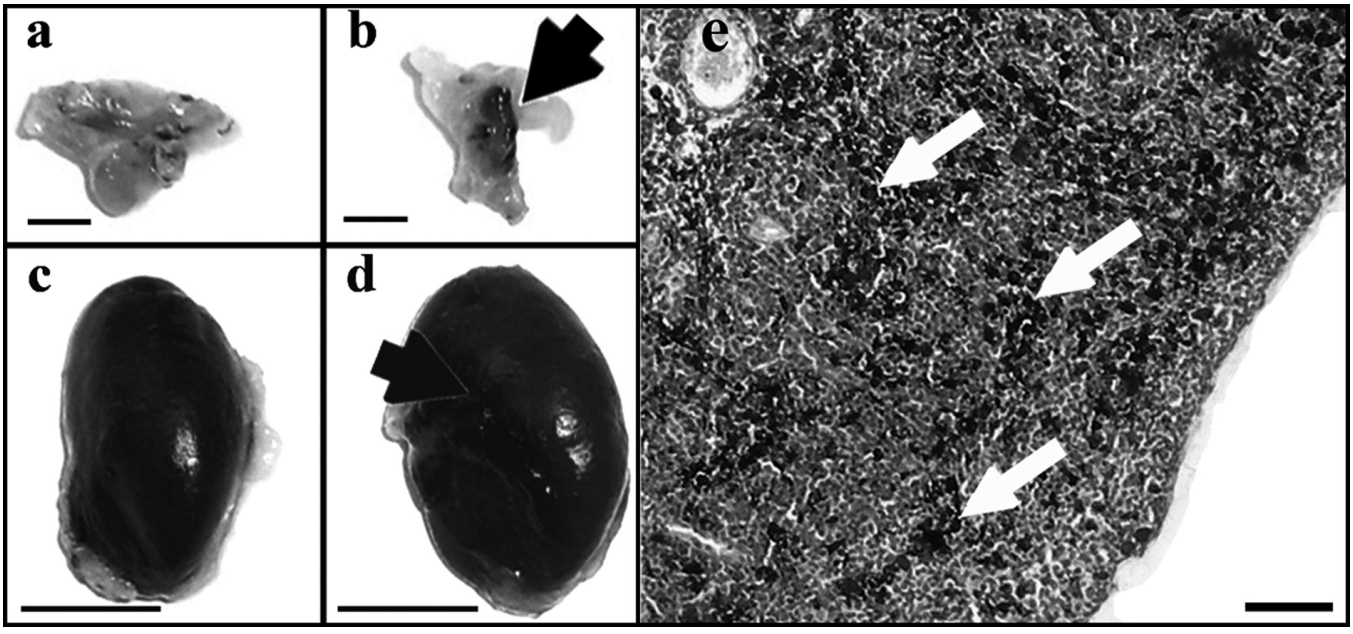

Fig. 8. Appearance of India ink in parathymic lymph nodes implanted under the kidney capsule of rat. Pelikan ink (10 μl) was dropped on a gelatin sponge that was placed under the kidney capsule of F344 rats. Saline (10 μl) dropped on gelatin sponge was placed under the kidney of control rats. Rats (~150g) were sacrificed after 24 h of implantation and parathymic lymph nodes (PLNs) were isolated. Sections were cut from PLNs isolated as described under Methods, stained with hematoxylin and viewed under a microscope. **a.** Control parathymic lymph nodes. **b.** India ink uptake in parathymic lymph nodes. **c)** Normal kidney. **d.** India ink under the capsule of kidney. Black arrows indicate the site of ink accumulation. **e.** Section showing the appearance of India ink traced 6 h after administration in the cortical region of the left parathymic lymph node. White arrows point to ink grains inside the lymph node. Bars: a, b, 0.5 cm; c, d, 1 cm; e, 100 μm.

generate metastases in the parathymic lymph nodes comes from the implantation of ink particles under the capsule of the kidney. Ink particles appeared within 6 h in the parathymic lymph nodes.

The research of parathymic lymph nodes has been neglected, contrary to their description in the 1960s (Miller, 1963; Bonney and Battenberg, 1967). Blau and Gaugas injected India ink intravenously, which concentrated in parathymic lymph nodes located inside the thymus capsule in mice. It is worth mentioning that parathymic lymph nodes sit on the surface of the thymus capsule in rats, surrounded by a fibrous capsule and brown adipose tissue, and can be separated from the thymus (Blau and Gaugas, 1968). The temporary interest in parathymic lymph nodes resurged when it was found that after acute gastroenteritis of rats the cells of exsudative ascites appeared in the parathymic glands (Steer and Foot, 1987). This finding directed attention to earlier experiments related to staining and X-ray contrast analysis of materials, which clarified that the lymphatic vessels of the peritoneal cavity perforate the diaphragm. Tilney has mapped the lymphatic system of rats in detail and has described that the lymph to the parathymic lymph nodes comes from the peritoneal cavity, liver, pericardium and from the thymus and pours its content

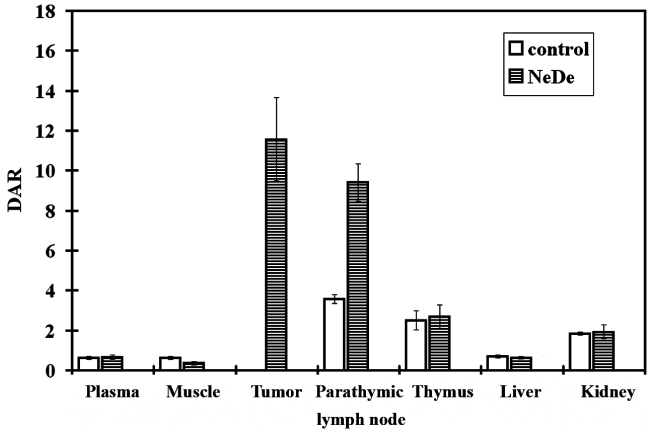

Fig. 9. Tissue distribution of radioactivity expressed in DAR after intravenous administration of ^{18}FDG in NeDe tumor-bearing rats. Metastatic potential of NeDe cells, plasma, muscle, tumor, parathymic lymph nodes, thymus, liver and kidney expressed as differential absorption ratio (DAR).

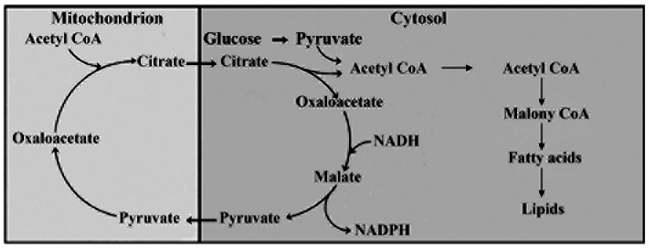

Fig. 10. Lipogenic pathway in NeDe tumor. In the mitochondria of tumor cells the terminal oxidation and the oxidative phosphorylation are not working under hypoxic conditions. In the absence of the normal aerobic metabolism the overproduction of acetylcoenzyme A induces fatty acid and lipid synthesis.

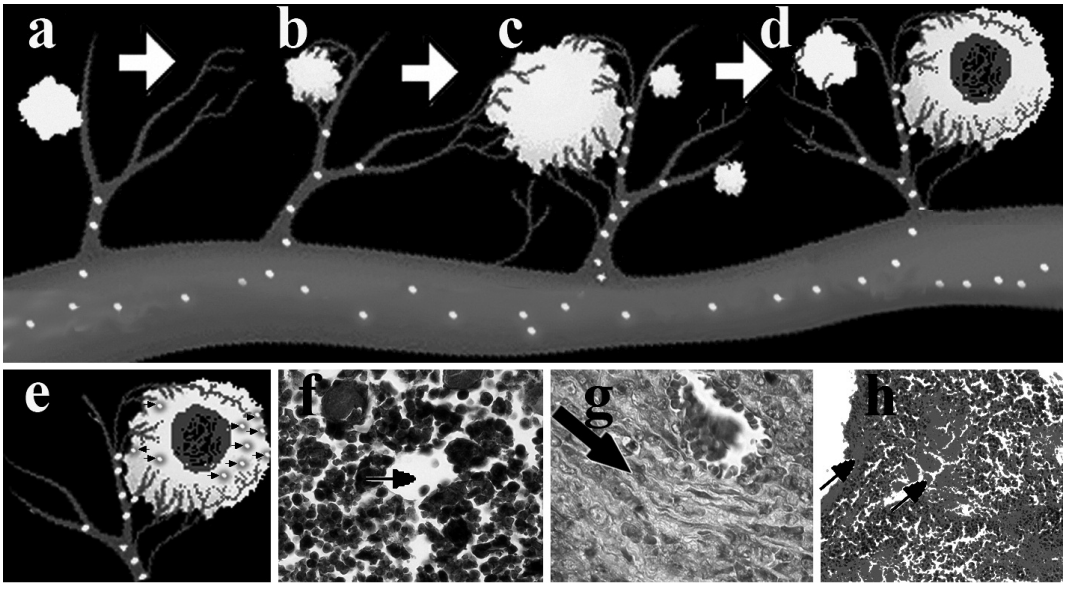

Fig. 11 Model for tumor development in vascularized and avascular tissue. **a-d**. The four stages of vascularization: **a.** Tumor cells seeded near a blood vessel. **b.** Beginning of angiogenesis in the small tumor. **c.** Intensive angiogenesis in growing tumor. **d.** Insufficent angiogenesis and necrosis inside the enlarged tumor. **e-h.** Avascular stages of metastasis formation: **e**. Disruptions in the primary tumor (small black arrows). **f.** Tumor and blood cells breaking away through the disrupted tumor (indicated by the black arrow). **g.** Detached cells enter the interstitial fluid, seen as white channels indicated by black arrow. **h.** The appearance of red blood cells (black arrows) in the parathymic lymph nodes indicate the formation of secondary tumors (metastases).

into the mediastinal lymph trunk (Tilney, 1971). Based on these observations it is logical to think that the metastatic cells of tumors growing under the kidney's capsule first enter the lymphatic vessels of the diaphragm, then, primarily through the parasternal lymphatic vessels, reach the parathymic lymph nodes. We assume that the capsule of the kidney and the parathymic lymph nodes constitute a complex similar to the Ranke complex after tuberculous infection, consisting of peripheral lung lesion with mediastinal lymph nodes. The Ranke complex at the time of its discovery contributed significantly to the understanding of the pathomechanism of the tuberculous infection. Based on this analogy we developed a relatively isolated system to study the formation of metastasis and to widen the range of the available metastatic models (Rowe et al., 1997; Zisman et al., 2003).

One can of course argue that the tumor growing under the capsule of the kidney may project metastatic cells to mesenteric lymph nodes as well, and detached tumor cells may reach the parathymic lymph nodes through the blood-vessels as referred to in the experiment of Blau and Gaugas (1968). Contrary to these objections we regard the kidney capsule-parathymic lymph node complex as an isolated system which provides an experimental approach for the future study of angiogenesis and the malignant transformation of parathymic lymph nodes.

The lipid droplet formation in the primary tumor also deserves some explanation. Lipogenesis in the tumor can be explained by the enhanced utilization of acetate and glucose in fatty acid synthesis (Medes et al., 1953). It was found that in tumor cells the normal aerobic metabolism turned to a highly glycolytic metabolism (Warburg et al., 1926). These findings indicated that the overproduction of acetylcoenzyme A from glucose could have caused fatty acid and subsequently lipid biosynthesis. The high aerobic glycolysis in tumor cells was explained by the glycolysis-citrate-lipogenesis pathway (Costello and Franklin, 2005). In this pathway glucose is glycolysed to pyruvate, which under aerobic conditions is turned to acetylcoenzyme A then to citrate in mitochondria. Tumor cells exhibit an increased citrate export from mitochondria to the cytosol (Parlo and Coleman, 1984, 1986). In the cytosol citrate is cleaved to acetylcoenzyme A and oxaloacetate by citrate lyase. Acetylcoenzyme A is then carboxylated to malonylCoA by acetylcoenzyme A carboxylase for fatty acid and cholesterol synthesis (Costello and Franklin, 2005). The pathway of lipid formation is depicted in Fig. 10. The lipid droplet formation we have visualized by Sudan black staining supports the idea that under hypoxic conditions the highly glycolytic metabolism of growing tumors leads to the deposition of the excess lipid.

Finally, we will discuss the relationship of angiogenesis to the formation of metastasis. The growth and spread of solid tumors are critically dependent on the induction of angiogenesis (Kayton et al., 1999). Convincing evidence suggests that tumor cells near the blood vessels grow in a vascularized fashion and co-opt existing blood vessels (Wesseling et al., 1994; Holmgren et al., 1995; Pezzela et al., 1997). It is also known that tumor cells seeded into avascular structures form tumors and metastases as small avascular structures, which induce the development of new vessels beyond a few millimetres in size (Folkman, 1971, 1990). This discrepancy indicates that the interplay between avascular systems and tumor-induced angiogenesis has not been explained satisfactorily. The formation of new blood vessels is the bottle-neck of tumor growth, as tumors need the supply of oxygen and nutrients for survival.

The results obtained by the NeDe tumor model offer some explanation as to how tumor spread may become a metastatic process. Due to insufficient angiogenesis at a critical size of the primary tumor, capillaries are disrupted and the blood enters the interstitial fluid. The inner part of the tumor is necrotised and ruptured at the cortical part (Fig. 11a-d). Tumor and blood cells are filtered through the kidney through a stream of interstitial channels, escape through the disruptions and enter the surrounding tissue. Tumor cells which have broken away enter the malformed cavernous venous and lymphatic capillaries containing large-channels and sinuses engorged with red blood cells. This idea is supported by the observation that a few days after tumor develeopment the PLNs did not contain erythrocytes, while after 12 days, the PLNs were stained with blood. Disruptions increase the volume of the interstitial tissue fluid. Networks of lymphatic capillaries located in the intercellular spaces collect the increased amount of tissue fluid containing tumor cells. Lymphatic capillaries merge with other lymphatics to eventually form lymph nodes. Lymph nodes are critical for the body's immune response as they filter the lymphatic fluid and store special cells that can trap cancer cells or bacteria that are traveling through the body in the lymph fluid. Interstitial fluid collected in small lymphatic vessels reaches the parathymic lymph nodes (Fig. 11e-h). Tumors growing under the kidney's capsule first enter the lymphatic vessels of the diaphragm, then, primarily through the parasternal lymphatic vessels, reach the parathymic lymph nodes. Lymphatic trunks reach the vascular system through the main thoracal lymph vessel (*ductus thoracicus*) that discharges lymph into the sublavian vein at the *angulus venosus*. As the vascular epithelial cells are normally resistant toward tumor invasion, the tumor cells flow back to the primary tumor (Fig. 11a-d, indicated by white dots in the circulation) and aggravate tumor formation near the primary tumor.

In summary, the results obtained with the new metastasis model indicate that: a) as a consequence of the lack of angiogenesis in the primary tumor, NeDe cells leave the blood vessels through the ruptures inside the primary tumor, b) blood cells and tumor cells enter the interstitial fluid, c) this fluid is collected by the lymphatic vessels inducing secondary tumor (primary

metastasis) indicated by the appearance of blood cells, India ink and tumor cells in parathymic lymph nodes and by the enormous increase in PTN size, d) tumor cells through the lymphatic system return to the vascular system and to the primary tumor and induce tertiary tumor (secondary metastasis) formation.

Acknowledgements. This work was supported by a grant of the Hungarian National Science and Research Foundation to G.B. (OTKA T42762 grant). The technical contributions by Gyongyi Hadhazi and Tamas Nagy are gratefully acknowledged.

References

Angevin E., Glukhova L., Pavon C., Chassevent A., Terrier-Lacombe M.J., Goguel A.F., Bougaran J., Ardouin P., Court B.H., Perrin J.L., Vallancien G., Triebel F. and Escudier B. (1999). Human renal cell carcinoma xenografts in SCID mice: tumorigenicity correlates with a poor clinical prognosis. Lab. Invest. 79, 879-888.

Blau J.N. and Gaugas J.M. (1968). Parathymic lymph nodes in rats and mice. Immunology 14, 763-765.

Bogden A.E., Haskell P.M., Le Page D.L., Kelton D.E., Cobb W.R. and Esber H.J. (1979). Growth of human tumor xenografts implanted under the renal capsule of normal immunocompetent mice. Exp. Cell. Biol. 47, 281-293.

Bonney W.M. and Battenberg J.D. (1967). Transthoracic thymectomy in rats. Transplantation 5, 544-546.

Costello L.C. and Franklin R.B. (2005). Why do tumour cells glycolyse?: from glycolysis through citrate to lipogenesis. Mol. Cell. Biochem. 280, 1-8.

Delahunt B. and Eble J.N. (1997). Papillary renal cell carcinoma: a clinicopathologic and immunohistochemical study of 105 tumors. Mod. Pathol. 10, 537-544.

Delahunt B., Eble J.N., McCredie M.R., Bethwaite P.B., Stewart J.H. and Bilous A.M. (2001). Morphologic typing of papillary renal cell carcinoma: comparison of growth kinetics and patient survival in 66 cases. Hum. Pathol. 32, 590-595.

Dezso B., Rady P., Morocz I., Varga E., Gomba S., Poulsen K. and Kertai P. (1991). Morphological and immunhistochemical characteristics of dimethylnitrosamine-induced malignant mesenchymal renal tumor in F344 rats. J. Cancer Res. Clin. Oncol. 116, 372-378.

Diaz Gomez M.I., Tamayo D. and Castro J.A. (1986). Administration of N-nitrosodimethylamine, N-nitrosopyrrolidine, or N'-nitroso-nornicotine to nursing rats: their interactions with liver and kidney nucleic acids from sucklings. J. Natl. Cancer Inst. 76, 1133-1136.

Fidler I.J. and Nicholson G.L. (1987) The process of cacer invasion and metastasis. Cancer Bull. 39, 126-131.

Folkman J. (1971). Tumor angiogenesis: therapeutic implications. N. Engl. J. Med. 285, 1182-1186.

Folkman J. (1990). What is the evidence that tumors are angiogenesis dependent? J. Natl. Cancer Inst. 82, 4-6.

Grossi F.S., Zhao X., Romijn J.C., ten Kate F.J. and Schroder F.H. (1992). Metastatic potential of human renal cell carcinoma: experimental model using subrenal capsule implantation in athymic nude mice. Urol. Res. 20, 303-306.

Guha A.K., Ghose T., Singh M., Aquino J., Blair A.H., Luner S.J. and Mammen M. (1991). Tumor localization of monoclonal antibodies against human renal carcinoma in a xenograft model. Cancer Lett. 61, 35-43.

Guyton K.Z. and Kensler T.W. (1993). Oxidative mechanisms in carcinogenesis. Brit. Med. Bull. 49, 523-544.

Hamacher K., Coenen H.H. and Stöcklin G. (1986). Efficient stereospecific synthesis of no-carrier-added 2-(^{18}F)-fluoro-2-deoxy-D-glucose using aminopolyether supported nucleophilic substitution. J. Nucl. Med. 27, 235-238.

Hard G.C. (1985). Differential renal tumor response to N-ethyl-nitrosourea and dimethylnitrosamine in the Nb rat: basis for a new rodent model of nephroblastoma. Carcinogenesis 6, 1551-1558.

Hard G.C. and Butler W.H. (1970). Cellular analysis of renal neoplasia: induction of renal tumors in dietary conditioned rats by dimethylnitrosamine, with a reappraisal of morphological characteristics. Cancer Res. 30, 2796-2805.

Hard G.C. and Butler W.H. (1971a). Ultrastructural study of the development of interstitial lesions leading to mesenchymal neoplasia in the rat renal cortex by dimethylnitrosamine. Cancer Res. 31, 337-347.

Hard G.C. and Butler W.H. (1971b). Ultrastructural analysis of renal mesenchymal tumor induced in rat by dimethylnitrosamine. Cancer Res. 31, 348-365.

Hard G.C. and Grasso P. (1976). Nephroblastoma in the rat: histology of a spontaneous tumor, identity with respect to renal mesenchymal neoplasms, and a review of previously recorded cases. J. Natl. Cancer Inst. 57, 323-329.

Hart I.R. and Saini A. (1992). Biology of tumor metastasis. Lancet 339, 1453-1457.

Hill R.P. (1992). Metastasis, Chapter 11. In: The basic sciense of oncology. Tannock I.F., Hill R.P., Bristow R.G. and Harrington L. (eds). McGraw-Hill, New York. pp 178-195.

Hillman G.G., Droz J.P. and Haas G.P. (1994). Experimental animal models for the study of therapeutic approaches in renal cell carcinoma. In Vivo 8, 77-80.

Holmgren L., O'Reilly M.S. and Folkman J. (1995). Dormancy of micrometastases: balanced proliferation and apoptosis in the presence of angiogenesis suppression. Nat. Med.1, 149-53.

Jasmin G. and Riopelle J.L. (1968). Of the DMN-induced epithelial tumors. Renal adenomas induced by dimethylnitrosamine. Enzyme histochemistry in the rat. Arch. Pathol. 85, 298-305.

Jiang F., Richter J., Schraml P., Bubendorf L., Gasser T., Sauter G., Mihatsch M.J. and Moch H. (1998). Chromosomal imbalances in papillary renal cell carcinoma: genetic differences between histological subtypes. Am. J. Pathol. 153, 1467-1473.

Kayton M.L., Rowe D.H., O'Toole K.M., Thompson R.B., Schwarz M.A., Stolar C.J. and Kandel J.J. (1999). Metastasis correlates with production of vascular endothelial growth factor in a murine model of human Wilms' tumor. J. Pediatr. Surg. 34, 743-747.

Khanna C. and Hunter K. (2005). Modelling metastasis *in vivo*. Carcinogenesis 26, 513-523.

Magee P.N. and Barnes J.M. (1962). Induction of kidney tumours in the rat with dimethylnitrosamine (N-nitroso-dimethylamine). J. Pathol. Bacteriol. 84, 19-31.

Marsden H.B. and Newton W.A. (1986). New look at mesoblastic nephroma. J. Clin. Pathol. 39, 508-513.

Medes G., Thomas A. and Weinhouse S. (1953). Metabolism of neoplastic tissue. IV. A study of lipid synthesis in neoplastic tissue slices *in vitro*. Cancer Res. 13, 27-29.

Miller J.F. (1963). Role of the thymus in immunity. Brit. Med. J. 2, 459-464.

Murphy G.P., Mirand E.A., Johnston G.S., Schmidt J.D. and Scott W.W. (1966). Renal tumors induced by a single dose of dimethylnitrosamine: Morphologic, functional, enzymatic, and hormonal characterizations. Invest. Urol. 4, 39-56.

Ono Y., Ito T., Tsujino S., Aizawa S. and Suzuki M. (1997). A study of papillary renal cell carcinoma. Clinicopathological, immunohistochemical features and its typing. Nippon Hinyokika Gakkai Zasshi. Jpn. J. Urol. 88, 587-595 .

Otto U., Huland H., Baisch H. and Kloppel G. (1984a). Transplantation of human renal cell carcinoma into NMRI nu/nu mice. II. Evaluation of response to vinblastine sulfate monotherapy. J. Urol. 131, 134-138.

Otto U., Kloppel G. and Baisch H. (1984b). Transplantation of human renal cell carcinoma into NMRI nu/nu mice. I. Reliability of an experimental tumor model. J. Urol., 131, 130-133.

Paragh G., Kertai P., Kovacs P., Paragh P., Fulop P. and Foris G. (2003). HMGCoA reductase inhibitor Fluvastatin arrests the development of implanted hepatocarcinoma in rats. Anticancer Res. 23, 3949-3854.

Paragh G., Foris, G., Paragh G., Seres I., Karanyi Z., Fulopp P., Balogh Z., Kosztaczky B., Teichmann F. and Kertai P. (2005). Different anticancer effects of fluvastatin on primary hepatocellular tumors and metastasis in rats. Cancer Lett. 222, 17-22.

Parlo R.A. and Coleman P.S. (1984). Enhanced rate of citrate export from cholesterol rich hepatoma mitochondria. J. Biol. Chem. 259, 997-1003.

Parlo R.A. and Coleman P.S. (1986). Continuous pyruvate carbon flux to newly synthesized cholesterol and the suppressed evolution of pyruvate generated CO_2 in tumors: further evidence for a persistent truncated Krebs cycle in hepatomas. Biochim. Biophys. Acta 886, 169-176.

Pezzela P., Pastorino U., Tagliabue E., Andreola S., Sozzi G., Gasparini G., Menard S, Gatter K.C., Harris A.L., Fox S., Buyse M., Pilotti S., Pierotti M. and Rilke F. (1997). Non-small-cell lung carcinoma tumor growth without morphological evidence of neo-angiogenesis. Am. J. Pathol. 151, 1417-1423.

Pulkkanen K.J., Parkkinen J.J., Kettunen M.I., Kauppinen R.A., Lappalainen M., Ala-Opas M.Y. and Yla-Herttuala S.C (2000). Characterization of a new animal model for human renal cell carcinoma. In Vivo 14, 393-400.

Rowe D.H., Kayton M.L., O'Toole K.M., Ingram M., Stolar C.J.H. and Kandel, J.J. (1999). Pathological angiogenesis in a murine model of human Wilms' tumor. 1999. J. Pediat. Surg. 34, 676-679.

Steer H.W. and Foot R.A. (1987). Changes in the medulla of the parathymic limph nodes of the rat during acute gastro-intestinal inflmmation. J. Anat. 152, 23-26.

Swann P.F. and McLean A.E.M. (1968). The effect of diet on the toxic and carcinogenic action of dimethylnitrosamine. Biochem. J., 107(Procs.), 14-15.

Terracini B. and Magee P.N. (1964). Renal tumours in rats following injection of dimethylnitrosamine at birth. Nature 202, 502-503.

Thomas C. and Schmahl D. (1964). Zur Morphologie der Nierentumoren bei der Ratte. Z. Krebsforsch. 66, 125-137.

Tilney N.L. (1971). Patterns of lymphatic drainage in the adult laboratory rat. J. Anat. 109, 369-383.

Trencsenyi G., Kertai P., Somogyi C., Nagy G., Dombradi Z., Gacsi M. and Banfalvi G. (2007). Chemically induced carcinogenesis affecting chromatin structure in rat hepatocarcinoma cells. DNA Cell Biol. 26, 649-655.

Trencsenyi G., Rozsa D., Bako F., Nagy G., Kertai P., Hunyadi J., Pocsi I., Muranyi E., Marian T. and Banfalvi G. (2009). Renal capsule parathymic lymph node complex: A new *in vivo* metastatic model in rats. Anticancer Res.(in press).

Uzvolgyi E., Katona A. and Kertai P. (1990). Tumor cell implantation with the use of Gelaspon gelatin sponge disc. Cancer Lett. 51, 1-5.

Warburg O., Wind F. and Negelein E. (1926). Über den Stoffwechsel von Tumoren in Körper. Klin. Woch. 5, 829-832.

Welch D.R. (1997). Technical considerations for studying cancer metastasis. Clin. Exp. Metastasis 15, 272-306.

Wesseling P., van der Laak J.A., de Leeuw H., Ruiter D.J. and Burger P.C. (1994). Quantitative immunohistological analysis of the microvasculature in untreated human glioblastoma multiforme. Computer-assisted image analysis of whole-tumor sections. J. Neurosurg. 81, 902-909.

Workman P., Twentyman P., Balkwill F., Balmain A., Chaplin D., Double J.A., Embleton J., Newell D., Raymond R., Stables J., Stephens T. and Wallace J. (1988). UK Coordinated Committee on Cancer Researc (UKCCCR) Guidelines for the welfare of animals in experimental neoplasia. Br. J. Cancer 77, 1-10.

Zisman A., Pantuck A.J., Bui M.H., Said J.W., Caliliw R.R., Rao N., Shintaku P., Berger F., Gambhir S.S. and Belldegrun A.S. (2003) LABAZ1: A metastatic tumor model for renal cell carcinoma expressing the carbonic anhydrase type 9 tumor antigen. Cancer Res. 63, 4952-4959.

Zoli W., Barzanti F., Dal Susino M., De Paola F., Tesei A., Ricotti L., Padovani F., Reno F. and Amadori D. (2002). Flow-cytometric determination of tumor cells in lymph nodes. Oncology 62, 128-135.

Accepted May 11, 2009